Volume, Surface, Connectivity and Size Distribution of Soil Pore Space in CT Images: Comparison of Samples at Different Depths from Nearby Natural and Tillage Areas

F. J. Muñoz-Ortega, F. San José Martínez, and F. J. Caniego Monreal

Abstract—The study of soil structure, i.e., the pores, is of vital importance in different fields of science and technology. Total pore volume (porosity), pore surface, pore connectivity and pore size distribution are some (probably the most important) of the geometric measurements of pore space. The technology of X-ray computed tomography allows us to obtain 3D images of the inside of a soil sample enabling study of the pores without disturbing the samples. In this work we performed a set of geometrical measures, some of them from mathematical morphology, to assess and quantify any possible difference that tillage may have caused on the soil. We compared samples from tilled soil with samples from a soil with natural vegetation taken in a very close area. Our results show that the main differences between these two groups of samples are total surface area and pore connectivity per unit pore volume.

1. Introduction

A soil matrix is commonly viewed as a hierarchical system made of primary and secondary particles (e.g., aggregates) of different sizes that shape soil pore space. Its structure is believed to be among the main factors controlling soil processes and functioning (Dexter 1988; Revil and Cathles 1999). In particular, important physical and biological processes within the soil–plant–microbial system, such as microbial population dynamics, nutrient cycling, diffusion, mass flow and nutrient uptake by roots, are affected by soil pore structure (Young and Crawford 2004).

Land use and management have long been known to affect soil structure (Gale and Cambardella 2000; Six *et al*. 2000; Lal 2002). Recent studies showed that contrasting land use and management practices can also lead to marked differences in soil pore structure (Peth *et al*. 2008; Kravchenko *et al*. 2011; Wang *et al*., 2012). Such differences can potentially affect processes within the soil matrix. It is well known that differences in land use and management generate notable changes in soil physical and hydraulic properties, including changes in soil organic matter content, soil porosity, hydraulic conductivity and water retention (Brye and Pirani, 2005).

Recent advances in X-ray CT of undisturbed soil columns provide 3D images of the soil interior (Saucier and Muller 1999; Gantzer and Anderson 2002; Posadas *et al*. 2003; Dathe *et al*. 2006; Gibson *et al*.2006; Nunan *et al*. 2006; Chun *et al*. 2008; San José *et al*. 2010, 2013). This is a significant step in characterizing heterogeneity of soil environments at micro-scales, as it allows obtaining exact information of the physical structure of the soil matrix.

Image analysis may be seen as a body of tools that facilitates extraction of quantitative information from images such as X-ray tomograms. Image analysis may be subdivided into five steps: display, filtering, segmentation, transformation and measurement of image features (Glasbey and Horgan, 1995). The display renders an array of pixels values as a picture on a computer screen. Filters enhance images by applying transformations based on groups of pixels to reduce noise and emphasize edges. Segmentation divides an image into regions that correspond to different objects or parts of objects. Morphological transformations are used to study the shape of objects. And measurements extract quantitative information from the enhanced images. Mathematical morphology (Serra 1982) is a theory that is based in the assumption that images consist of structures that

may be handled by set theory. It provides useful morphological transformations and measurement procedures for quantifying the geometry of images (San José *et al.* 2013 and references therein).

The objectives of this study are to characterize the geometry of the soil pores by using several geometric 3D image measurements. The second objective is to evaluate whether different soil management (natural vegetation vs. tillage) as well as the depth at which sample was taken, exhibit significantly different geometric measurements. Finally, we study how these measures are related and how these measures relate to soil type and depth at which samples were taken.

2. Theory: Morphological Image Analysis

The theory of mathematical morphology provides a number of tools that allow us to characterize geometric objects, such as the background components of a binary image (the set of pixels with value 1), called objects. The fundamental concepts of mathematical morphology are morphological transformations; they change the size or the shape of the object under study. A quantitative description of the object is obtained from the measurement of a functional (e.g., volume) over the object properly transformed. Morphological transformations are formulated in the language of set theory in which, for a binary image, these sets correspond to the objects (set of pixels with value 1) in the image. To morphologically transform a set A another set B is needed, usually a sphere, which is called a structuring element. The basic morphological transformations are two: dilation and erosion. If we call B^d as the structuring element with size d then the dilation of A is defined as:

$$\mathrm{Dil}(A)_d = \{x - y : x \text{ in } A,\ y \text{ in } B^d\}$$

The main effect of dilation of A is an "expansion" of the boundary of A. The erosion of A is defined as:

$$\mathrm{Ero}(A)_d = \{x \text{ in } R^n : (B^d + x) \text{ subset } A\}$$

where R^n is the n-dimensional Euclidean space where the objects are defined. The main effect of erosion on A is the "contraction" of the border of A. Another transformation is morphological opening which is a combination of the two basic operations. The opening of A by B^d is defined as:

$$\mathrm{Op(A)}_d = \mathrm{Dil}(\mathrm{Ero}(A)_d)_d$$

The effects of the opening of A is the smoothing of contours, the breaking of narrow necks and the removal of small objects (objects with size smaller than the size of the structuring element). If the set on which the opening operation is performed is formed by components of different sizes (like the pores on a porous medium image) then a sequential use of the morphological opening with increasing sizes of the spherical structuring element simulates a process of "sieving," since for each structuring element size all the smaller components disappear after the operation (see Fig. 1). This procedure is usually called morphological granulometry and, following Vogel (2002), in the study of porous media images the size criteria used almost perfectly reflects the idea of the hydraulic diameter of a pore. A functional measurement such as the volume, expressed in relation to the size of the structuring element d, provides a measure of the distribution of the functional in the set. Therefore, for an image of a porous medium a function of pore size distribution can be defined (Vogel, 2002) as:

$$F(d) = \mathrm{Vol}(\mathrm{Op}(A)_d)$$

for differents values of d. Where *Vol* means volume.

3. Materials and Methods

3.1. Soil Study and Sampling

Undisturbed soil samples were taken in December 2008 in two nearby areas within the experimental farm "El Encín" this farm belongs to the Instituto Madrileño de Investigación y Desarrollo Rural Agrario y Alimentario (IMIDRA) located in Alcala de Henares, Madrid, Spain. The first sampled area (labeled *T*), with coordinates (WGS84) 40°31′29″N, 3°17′30″W, is an agricultural area which at the time of sampling had a cotton crop (Gossypium sp.). Soil in this area was identified (INIA, 1977) as Calcic Haploxeralf, adapted to the USDA classification (Soil

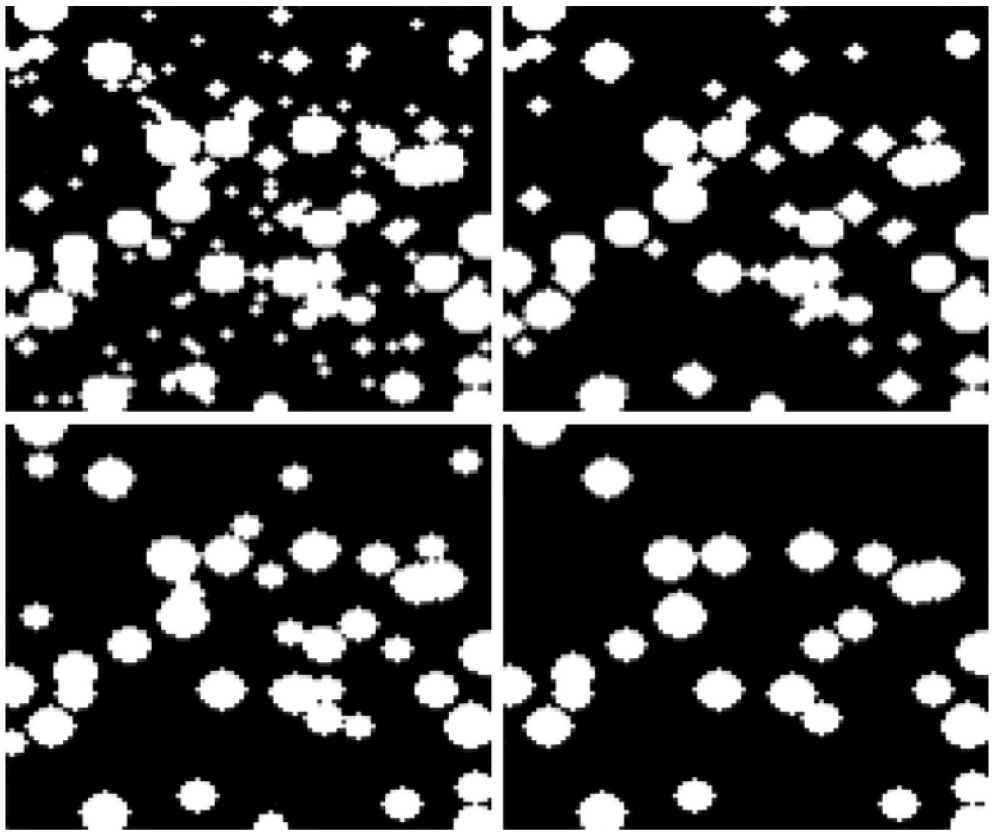

Figure 1
Example of the effect of morphological granulometry on an image of a medium consisting of objects of different sizes. In the different stages of the process it can be seen that the objects disappear according to its increasing size

SURVEY STAFF 2010); the textural family of the soil is clay loam with the following proportions: 3.4 % sand, 35.8 % silt, 60.8 % clay and 1.62 % organic matter. The second sampled area (labeled *N*), with coordinates (WGS84) 40°31′6″N, 3°17′21″W, is a natural site located on a terrace of the Henares river with riparian vegetation (Tamarix sp., Ulmus sp.). Soil in this second area was identified (INIA, 1977) as typic xerofluvent, adapted to the USDA classification (SOIL SURVEY STAFF 2010); the textural family of the soil is silty clay loam with the following proportions: 12.3 % sand, 60.8 % silt, 26.9 % clay and 0.85 % organic matter.

In order to extract and preserve the undisturbed samples methacrylate cylindrical containers were used and they were introduced directly into the soil by manual drilling. The dimensions of the containers are: 3 cm high, 2.6 cm inner diameter and 2 mm thickness. Soil samples were taken at three depths about 10 cm apart, the first group of samples being flush with the surface. In total 24 samples were extracted, 12 of each soil type with a total of 4 replicates in each of the three depths sampled in each area.

3.2. Image Acquisition and Processing

Soil samples were scanned using an X-ray CT scanner at the Gregorio Marañon Hospital's Laboratory of Medical Imaging and Experimental Medicine in Madrid (Spain). The tomograph used an energy of 50 keV for scanning the samples. The output data obtained after the reconstruction phase is a set of 3D unsigned 16-bit RAW images. The size of the images are 1,392 slices, each slice with 1,600 $\times$ 1,600 pixels. The spatial resolution of the images is 0.03 mm/pixel side. The spacing between sections is 0.03 mm so the 3D image has the same resolution in all three

Table 1

Labeling of images obtained according to the sampling area

	Area *T* (tillage)	Area *N* (natural)
0 cm (surface)	*T*1_1, *T*1_2, *T*1_3	*N*1_1, *N*1_2, *N*1_3, *N*1_4
−10 cm	*T*2_1, *T*2_2, *T*2_3, *T*2_4	*N*2_1, *N*2_2, *N*2_3, *N*2_4
−20 cm	*T*3_1, *T*3_2, *T*3_3, *T*3_4	*N*3_1, *N*3_2, *N*3_3

spatial directions. Due to an error in the acquisition/reconstruction of data only 22 of the 24 samples have a final reconstructed image. Table 1 summarizes labeling of the images obtained according to the sampling area. This labeling is of the form *Ln*1_*n*2 where *L* is the treatment: *T* (tillage) or *N* (natural), *n*1 is the depth 1 (shallow), 2 (intermediate), 3 (the deepest) and *n*2 is the repetition.

Image processing was performed with the public domain program ImageJ version 1.47 v developed at the National Institute of Health (RASBAND 1997). The image format was changed from RAW to TIFF.

The first image processing was thresholding (segmentation) in order to classify the entire set of pixels of the image into two regions, the region of interest (foreground) and the region of background. The foreground in this work corresponds to the porous phase of the sample and the background region corresponds to the solid phase.

A local (adaptive) thresholding algorithm was used to implement the process of thresholding. It has been shown that these types of algorithms are stable

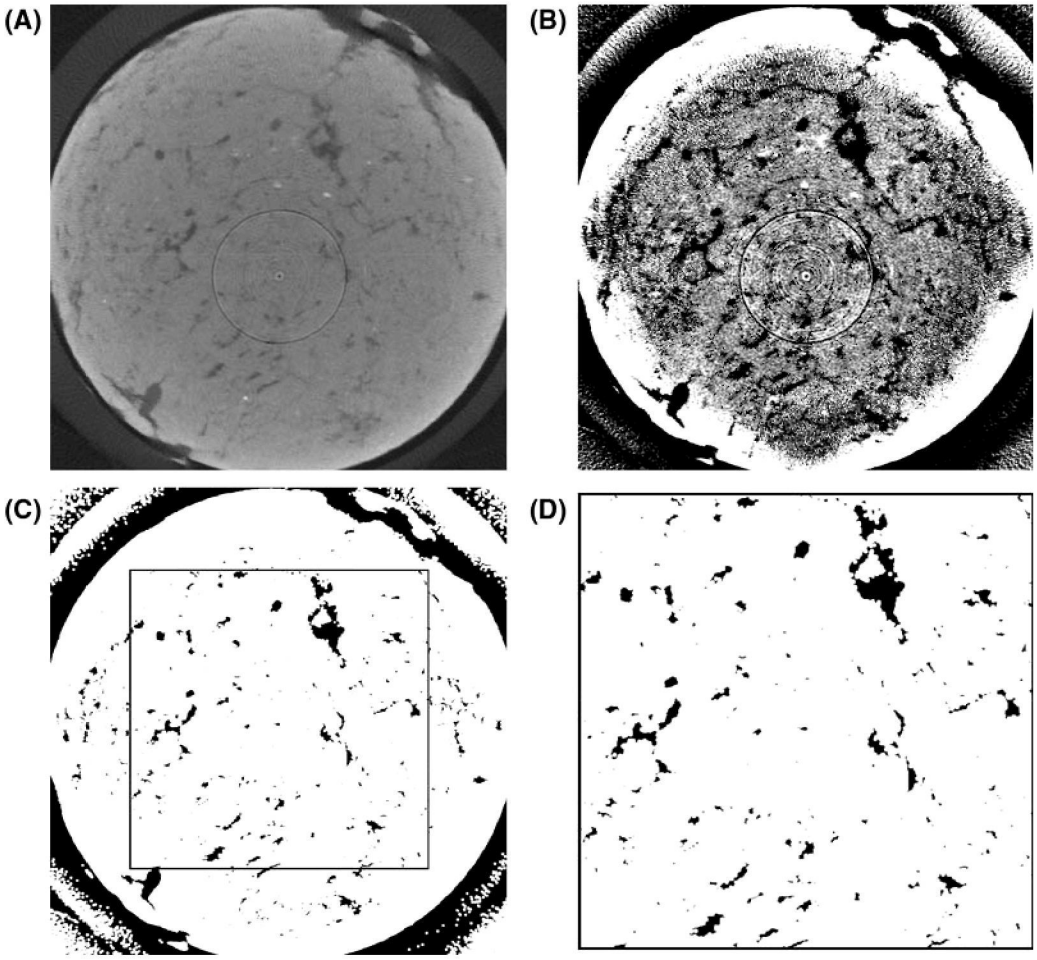

Figure 2
Procedure performed on *T*2_2 sample. **a** Image acquisition; **b** local threshold; **c** maximum filtering; **d** resampling

and are precise (Iassonov 2009). The local segmentation algorithm used is based on the mean operation. Thresholding works as follows: for each pixel of the image a threshold is calculated; if the pixel value is below the threshold then the pixel is classified as background, otherwise it is classified as an object (foreground). Calculation of the threshold for each pixel is made by examining pixel values of the surroundings of the pixel to be replaced. For this work the surroundings have been chosen for a given radius of 100 pixels which corresponds to an actual sample size of 3 mm. Figure 2b shows the result of applying this thresholding on the original image of Fig. 2a.

Images were filtered in order to reduce Gaussian noise and artifacts. These imperfections arise during the tomographic scan due to defects in the X-ray beam and the detector used (observe the concentric ring-shape structures on the inside of the sample in Fig. 2a). The filter chosen was the spatial filtering that uses the maximum function with a radius of action r equal to 2 pixels. The filtering operation operates on each image pixel as follows: each pixel x in the original image is replaced by the maximum of the values of the pixels covered by the ball of radius r when it is centered on the pixel x. Figure 2c shows the result of this filter where it can see that the noise and ring artifacts have disappeared.

An inner region with cubic shape of size $512 \times 512 \times 512$ pixels was selected from each 3D picture for the study of the geometric characteristics. This region corresponds to a cube whose edge has an actual length of 15.36 mm. This size was chosen to avoid taking pixels of the sample container or of soil at the perimeter. Figure 2c shows a section of the region where it will resample the marked square. Figure 2d shows the results of resampling.

3.3. Computation of Geometrical Features

Total pore surface, specific pore surface, total pore connectivity, specific pore connectivity, proportion of macropores (POM) and pore size distribution was calculated for each image.

For the computation of porosity, pore surface (total and specific) and connectivity (total and specific) we used computer code developed in Michielsen and De Raedt 2001; the authors describe a method for calculating the volume, surface and connectivity of an object in a 3D digital image. The authors compute the number of pixels (n_c), the number of vertices (n_v), the number of edges (n_e) and the number of faces (n_f) of the object in the image, so that:

$$\begin{aligned} \text{Volume} &= n_c \\ \text{Surface} &= -6 \cdot n_c + 2 \cdot n_f \\ \text{Connectivity} &= -n_c + n_f - n_e + n_v \end{aligned}$$

In this way porosity is obtained by dividing the volume of the object (in our case the object is the set of pores) by the total volume of the image (the product of its dimensions $512 \times 512 \times 512$). The total pore surface (mm^2) was obtained by multiplying the surface calculated in this method by the square of the resolution surface, and the specific pore surface (mm^{-1}) by dividing total pore surface by the volume of the object expressed in mm^3 (i.e., multiplied by the cube of the resolution). Total connectivity corresponds to the connectivity obtained in the program and specific connectivity (mm^{-3}) is obtained by dividing the total connectivity by the volume of the object expressed in mm^3.

For the distribution of pore sizes in this work we followed the process of morphological granulometry (Vogel 2002), where the size of a spherical structuring element that has been used follows the sequence: 1, 3, 5, 7, ... (pixels) that correspond to equivalent pore diameters given in μm of 30, 90, 150, 210, ...

POM is defined as the percentage of pores with a diameter >75 μm (Brewer 1964); in this paper POM corresponds to the sum of the relative frequencies of pore volumes with a diameter greater than or equal to 3 pixels.

3.4. Statistics

Statistical analyzes were performed on the variables porosity, POM, total pore surface (mm^2), specific pore surface (mm^{-1}), total pore connectivity (dimensionless) and specific pore connectivity (mm^{-3}) taking treatment (soil use) and sample depth into account. Statistical analysis utilized Statgraphics Centurion XVI (StatPoint Technologies, Inc.) has

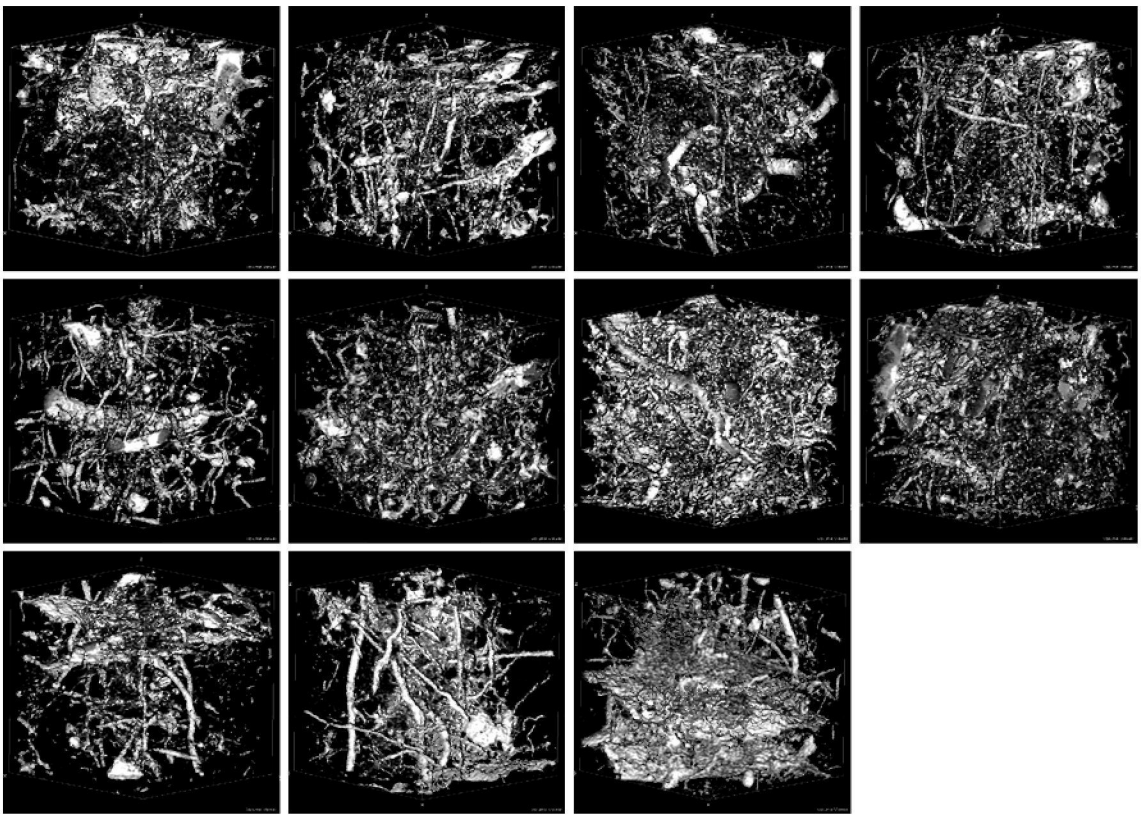

Figure 3
3D reconstructions of natural soil samples (*N*)

been used. Significance tests for the evaluation of the effects of the treatment factors and depth have been performed using the ANOVA multifactorial analysis for all variables. The ANOVA test evaluates factors that have a statistically significant effect on each dependent variable. ANOVA analysis for the contribution of each factor is measured by the sum of squares Type III which is measured by removing the effects of other factors. Pearson correlations between each pair of variables have been measured for the entire set of data (not rated by factors) in order to evaluate whether there are correlations significantly different from zero.

Comparisons between pairs of pore size distributions was performed using the Kolmogorov–Smirnov test for paired data sets, using the program MATLAB R2010a (MathWorks, Inc.). This test assumes as a null hypothesis that the two distributions of data sets come from the same continuous distribution and measures the maximum distance between the cumulative distributions for each value of the distribution.

4. Results and Discussion

4.1. Visualization of Pore Space

Figures 3 and 4 show three-dimensional reconstructions of pore space in 22 soil samples. In general, it seems to us that *N* samples have more pores than *T*. In addition, in the natural soil (Fig. 3) the samples *N*1_1, *N*2_3, *N*2_4 and *N*3_3 show a high porosity; the *N* samples indicate a large number of tube-shaped pores crossing the sample mainly from top to bottom; the pores clearly appear to have a biological origin. Tilled soil samples *T*1_1, *T*2_2, and *T*3_1 (Fig. 3) have a high porosity; however, *sample* *T*2_3 appears to have very little as many tubular pores are observed, similar to the natural soil. The

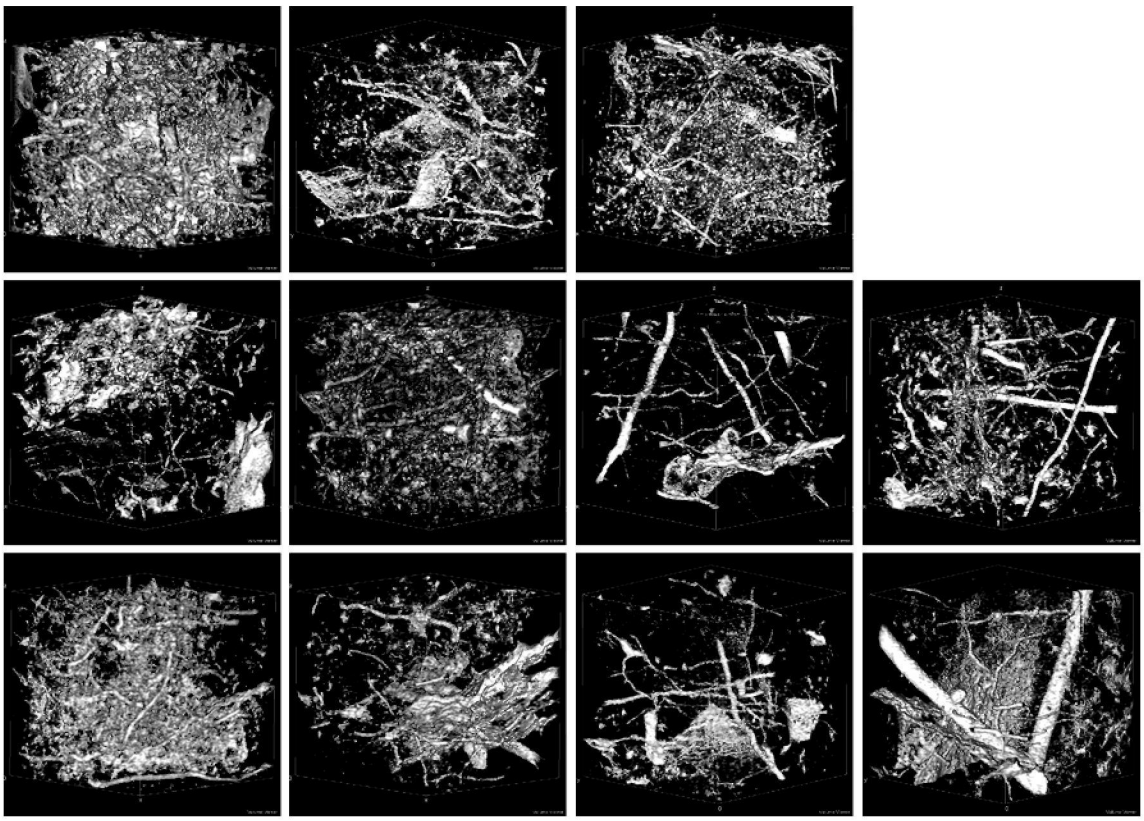

Figure 4
3D reconstructions of tilled soil samples (*T*)

largest pores were observed in *sample* *T*3_4. The direction of the pores in tilled soil does not seem as clear as in the natural soils.

4.2. *Porosity, Surface, Connectivity and Proportion of Macropores*

Table 2 lists the characteristics [porosity, POM, total pore surface (mm^2), specific pore surface (mm^{-1}), total pore connectivity (dimensionless) and specific pore connectivity (mm^{-3})] for all soil samples with the mean values and standard deviations of each group of data.

In the second column of Table 2 corresponding to porosity it can be seen that greater porosity occurs in the sample *T*1_1 (11.071 %). However, on average, pores are greater for *N* samples (5.333 %) compared to *T* samples (3.071 %). As observed by visual analysis of the reconstructions (Sect. 4.1), high porosity natural treatment samples are *N*1_1, *N*2_3, *N*2_4 and *N*3_3 and *N*1_3; *T*1_1, *T*2_2 and *T*3_1 have the greatest porosity among the tillage treatment samples. Small differences in porosity show a decrease with depth; for *T* the porosity is higher in the surface samples (4.766 %) than in the other depths (2.424 and 2.444 %). In *N* samples the average porosity is 3/10 higher in the intermediate depth (5.910 %) than in the surface (5.686 %) and these two are greater than the mean of the deepest group (4.093 %).

If we relate data porosity with POM it can be seen that the samples with greater porosity (e.g., *T*1_1) have a high POM (0.897). Moreover, this sample has the greatest POM; therefore, it seems that higher porosity is due to pores having a large size and not to a high amount of smaller pores (this can be checked with the value of total pore connectivity which increases with the number of pores and decreases with the number of tunnels). Smaller values of POM are at about 0.5 (samples *T*1_2, *T*2_3, *T*2_4 and *T*3_3).

Table 2

Characteristics of all soil samples analyzed for the two treatments and the three different levels of depth

Sample	Porosity (%)	POM	Sup total (mm^2)	Sup/volPoro (mm^{-1})	Total connectivity (adim)	Specific connectivity (mm^{-3})
*T*1_1	11.071	0.897	8,011.390	19.969	13,283.000	33.110
*T*1_2	0.810	0.520	1,811.018	61.677	27,851.000	948.509
*T*13	2.416	0.640	4,676.020	53.405	39,536.000	451.541
Mean *T*1	4.766	0.686	4,832.809	45.017	26,890.000	477.720
SD *T*1	5.519	0.192	3,103.158	22.083	13,152.857	458.261
*T*2_1	2.958	0.762	3,721.219	34.709	16,770.000	156.419
*T*2_2	4.450	0.777	6,066.432	37.614	24,029.000	148.990
*T*2_3	0.915	0.592	1,732.554	52.224	9,740.000	293.593
*T*2_4	1.373	0.563	2,821.415	56.689	19,019.000	382.135
Mean *T*2	2.424	0.673	3,585.405	45.309	17,389.500	245.284
SD *T*2	1.610	0.112	1,843.066	10.784	5,933.994	112.889
*T*31	3.292	0.692	5,691.022	47.700	22,772.000	190.868
*T*3_2	2.982	0.730	4,095.443	37.902	13,415.000	124.151
*T*3_3	0.924	0.585	1,761.242	52.600	11,823.000	353.099
*T*3_4	2.578	0.771	3,280.464	35.110	15,267.000	163.399
Mean *T*3	2.444	0.694	3,707.043	43.328	15,819.250	207.879
SD *T*3	1.055	0.080	1,638.611	82.07	4,844.108	100.610
Mean *T*	3.071	0.684	3,969.838	44.509	19,409.545	295.074
SD *T*	2.896	1.260	2,015.107	12.390	8,705.074	250.801
*N*1_1	9.137	0.821	9,453.758	28.552	7,626.000	23.032
*N*1_2	3.729	0.700	5,814.484	43.026	28,244.000	208.998
*N*1_3	5.487	0.782	6,637.091	33.379	23,543.000	118.402
*N*1_4	4.389	0.750	5,953.207	37.429	27,939.000	175.656
Mean *N*1	5.686	0.763	6,964.635	35.596	21,838.000	131.522
SD *N*1	2.412	0.051	1,697.926	6.140	9,715.057	81.430
*N*2_1	3.432	0.750	4,493.565	36.130	17,403.000	139.926
*N*2_2	4.406	0.710	6,810.233	42.655	20,338.000	127.385
*N*2_3	8.601	0.800	10,056.866	32.264	1,226.000	3.933
*N*2_4	7.199	0.776	9,049.522	34.687	13,765.000	52.762
Mean *N*2	5.910	0.759	7,602.547	36.434	13,183.000	81.002
SD *N*2	2.402	0.039	2,477.293	4.443	8,412.510	64.189
*N*3_1	4.546	0.806	5,081.254	30.846	27,936.000	169.584
*N*3_2	2.778	0.723	4,124.254	40.961	20,925.000	207.824
*N*3_3	4.956	0.768	6,236.258	34.723	22,459.000	125.049
Mean *N*3	4.093	0.766	5,147.255	35.510	23,773.333	167.486
SD *N*3	1.157	0.041	1,057.548	5.104	3,685.666	41.427
Mean *N*	5.333	0.762	6,700.954	35.877	19,218.545	122.959
SD *N*	2.095	2.067	2,001.703	4.758	8,706.446	69.978

It should be noted that these are *T* samples and indicate a ratio of approximately 50 % of macropores. For *N* samples, the values are in the range 0.700–0.821, so the minimum POM in these samples is 70 %; therefore, as can be observed in the group mean values, POM in *N* samples is greater than in *T* samples.

Surface samples indicate that, although in terms of absolute total pore surface (mm^2) the highest values on average correspond to *N* samples (6,700.9 in *N* vs. 3,969.8 in *T*), in relative terms the size of pores and specific pore surface (mm^{-1}) in *T* samples are higher (44.509 in *T* vs. 35.877 in *N*); all mean values in *T* samples are greater than 43 mm^{-1} while all averages values for *N* are below 37 mm^{-1}. This suggests that, although there are more pore surfaces in *N*, the specific surface area per pore volume is greater in *T*; that is, for the same volume of pores, pores in *T* samples provide the largest surface area. This can be interpreted as the pores in *T* samples are irregular or there are a great number of small pores (except for *T*1_1). The latter interpretation is in agreement with the POM data; connectivity data can be used to test it.

Table 3

Pearson correlations between each pair of variables to the entire set of samples

	Porosity	POM	Total pore surface	Specific pore surface	Total pore connectivity	Specific pore connectivity
Porosity	1	0.826***	0.9143***	−0.8182***	−0.3723*	−0.6632***
POM	0.826***	1	0.743***	−0.9841***	−0.2462	−0.8294***
Total pore surface	0.9143***	0.743***	1	−0.6931***	−0.2569	−0.6759***
Specific pore surface	−0.8182***	−0.9841***	−0.6931***	1	0.3405	0.8264***
Total pore connectivity	−0.3723	−0.2462	−0.2569	0.3405	1	0.4575**
Specific pore connectivity	−0.6632***	−0.8294	−0.6759***	0.8264***	0.4575**	1

* <0.1, ** <0.05, *** <0.001

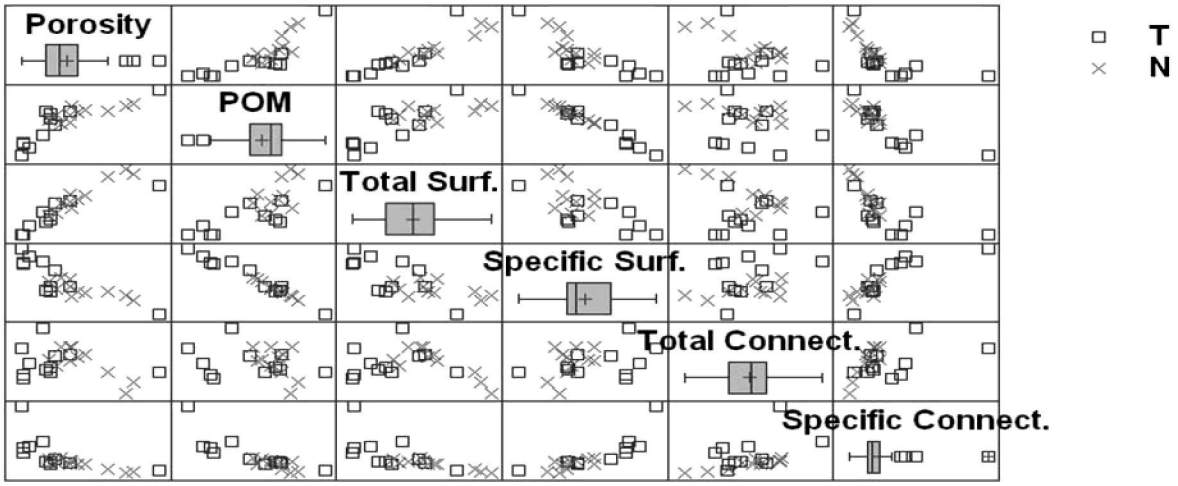

Figure 5
Dispersion matrix that shows possible correlations between groups of samples

In absolute terms, the two treatments on average have approximately the same total pore connectivity (dimensionless), around 19,000. To know which is more connected it is recalled that a sample will be more connected, have more tunnels, branches and closed loops when its connectivity value is lower. The *T*1_3 sample exhibits an extreme value of this total connectivity, resulting in a high positive value (39,536.00). This indicates a high number of connected components (isolated pores) and/or a small value of tunnel branches and loops. The *N*2_3 sample has the minimum value of total pore connectivity (dimensionless) (1,226.00) In the same way that high porosity is visualized in the sample we think that all this porosity forms a low value of connected components and most of the branches and loops are connected. For *T*1_1, which has a high POM and a high value of porosity, since its connectivity is low it may indicate that porosity is due to a few number of large pores (which can have many ramifications and tunnels) and is not due to a higher amount of smaller pores (which would increase the value of connectivity).

Regarding surface values, pores in *T* samples are either more irregular or are smaller and more numerous (this second option is more consistent with the POM data) and specific connectivity in *T* samples is greater than in *N* samples (i.e., for an equal volume of pores, pores in *N* either have fewer components or have more branches versus pores in *T* samples in which many disconnected (without branching structures form) pores appear (without branching structures).

Table 3 shows the relationship between each pair of variables measured for the entire set of samples quantified by Pearson correlations. Figure 5 shows

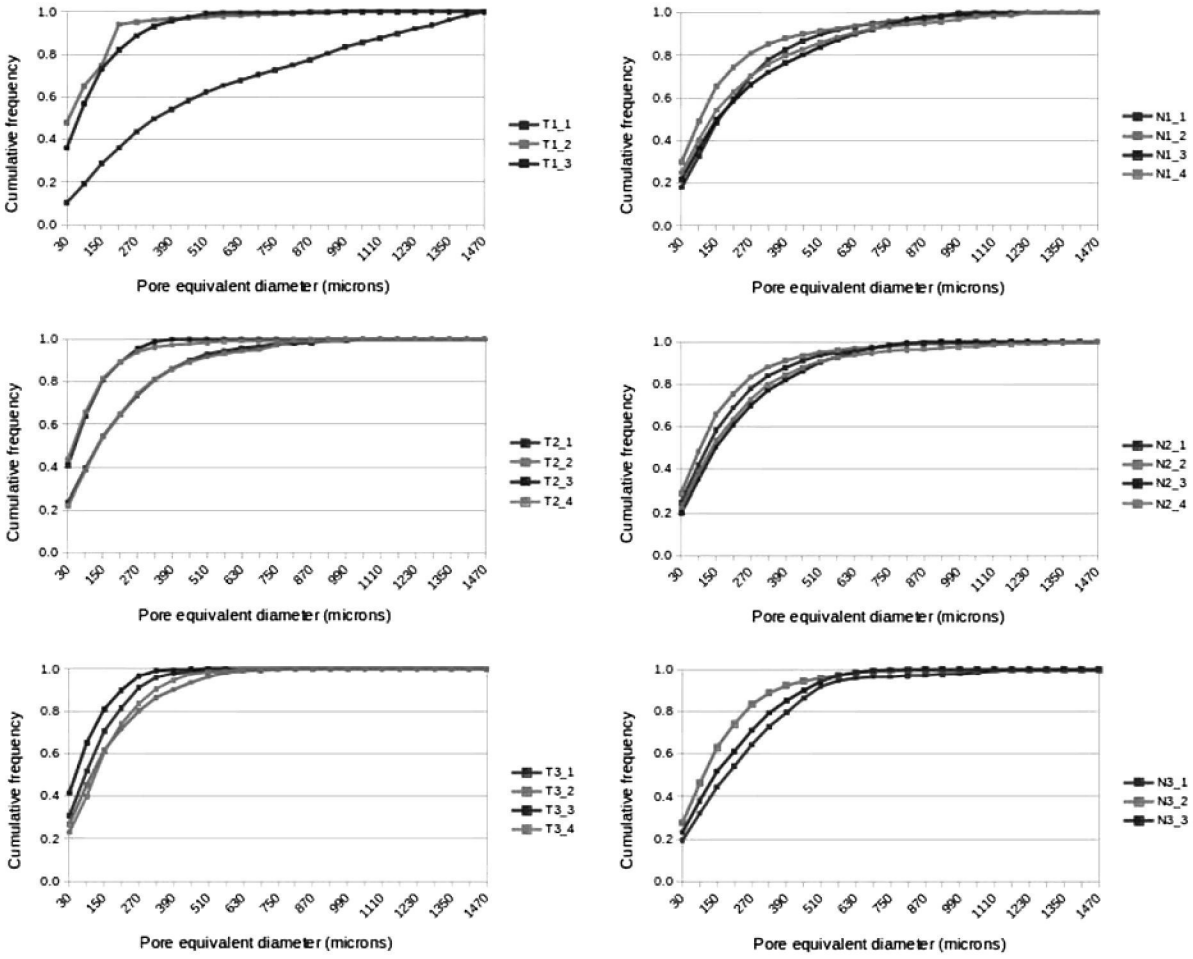

Figure 6
Distribution of cumulative relative frequencies of pore size for each group of samples, expressed in terms of equivalent diameter (μm)

the scatter plots of these relationships, identifying samples of each treatment. Significant relationships found at a confidence level of 95 % are listed following Table 3.

- Porosity and total pore surface: as expected, the higher porosity, the higher the pore surface.
- Porosity and specific pore surface: this relation is negative; the greater porosity, the lower the pore surface. This relationship is also expected because when the pores are larger the surface area per unit volume of pore is lower. Moreover when the number of pores is increased it begins to coalesce and share walls so that the surface pores decreases.
- Specific pore connectivity and specific pore surface: for a given pore, the more irregular the pore is, the more branches and loops it has and, hence, greater surface.
- Porosity and POM: a higher porosity in absolute terms correlates to a higher proportion of large pores.
- Total pore surface and POM: if there is greater surface area of pores there is a higher proportion of large pores.
- Total pore surface and specific pore surface: this relation is negative; a higher total pore surface area correlates with a smaller pore surface area per unit area. That is, if there are more pores they are more regular and/or larger and, hence, its specific surface area is smaller.
- Total pore connectivity and specific pore connectivity: the less connected a pore is the less connected the total is.

Table 4

*Statistical results of the Kolmogorov–Smirnov test in comparison of pairs of distributions with * if $P < 0.1$, ** if $P < 0.05$ and *** if $P < 0.01$*

	T1_1	T1_2	T1_3	T2_1	T2_2	T2_3	T2_4	T3_1	T3_2	T3_3	T3_4	N1_1	N1_2	N1_3	N1_4	N2_1	N2_2	N2_3	N2_4	N3_1	N3_2
T1_2	0.840***																				
T1_3	0.640***	0.200																			
T2_1	0.640***	0.360*	0.280																		
T2_2	0.520***	0.360*	0.240	0.120																	
T2_3	0.760***	0.320	0.360*	0.400**	0.360*																
T2_4	0.760***	0.160	0.200	0.280	0.280	0.360*															
T3_1	0.720***	0.120	0.160	0.320	0.280	0.200	0.160														
T3_2	0.600***	0.240	0.120	0.200	0.160	0.280	0.160	0.160													
T3_3	0.760***	0.280	0.320	0.400**	0.360*	0.080	0.320	0.160	0.240												
T3_4	0.680***	0.200	0.240	0.280	0.200	0.160	0.240	0.120	0.120	0.200											
N1_1	0.560***	0.400**	0.400**	0.160	0.200	0.560***	0.400**	0.360*	0.280	0.480***	0.400**										
N1_2	0.640***	0.400**	0.280	0.120	0.120	0.400**	0.360*	0.360*	0.240	0.400**	0.240	0.160									
N1_3	0.440**	0.480***	0.320	0.200	0.160	0.440**	0.400**	0.400**	0.240	0.440**	0.320	0.160	0.200								
N1_4	0.520***	0.480***	0.400**	0.200	0.240	0.560***	0.400**	0.440**	0.360*	0.560***	0.400**	0.160	0.160	0.120							
N2_1	0.640***	0.360*	0.280	0.080	0.120	0.360*	0.280	0.320	0.200	0.400**	0.200	0.200	0.120	0.240	0.200						
N2_2	0.640***	0.360*	0.280	0.160	0.160	0.400**	0.280	0.320	0.200	0.400**	0.280	0.200	0.240	0.280	0.320	0.160					
N2_3	0.520***	0.360*	0.280	0.120	0.200	0.520***	0.280	0.320	0.280	0.480***	0.400**	0.160	0.160	0.160	0.280	0.200	0.200				
N2_4	0.600***	0.400**	0.520***	0.280	0.360*	0.680***	0.440**	0.480***	0.440**	0.640***	0.560***	0.160	0.320	0.280	0.200	0.360*	0.280	0.320			
N3_1	0.600***	0.320	0.360*	0.120	0.200	0.520***	0.360*	0.320	0.240	0.480***	0.360*	0.160	0.160	0.200	0.240	0.160	0.160	0.160	0.200		
N3_2	0.680***	0.280	0.160	0.160	0.160	0.320	0.200	0.160	0.120	0.320	0.160	0.240	0.200	0.240	0.320	0.160	0.200	0.240	0.400**	0.240	
N3_3	0.600***	0.280	0.160	0.160	0.120	0.280	0.240	0.200	0.120	0.240	0.160	0.280	0.200	0.240	0.360*	0.160	0.160	0.240	0.400**	0.240	0.120

- Specific pore surface and POM: this relation is negative; when there are pores with a high specific surface value then small pores are more abundant. That is, the greater specific surface areas are small.

4.3. Pore Size Distribution

Figure 6 shows the cumulative relative frequency distribution of pore sizes in each group of samples. These distributions are expressed as a function of equivalent pore diameters obtained from the morphological opening radius used at each stage of morphological granulometry. It can be seen that the *N* treatment samples exhibit similar behavior: All start between 20 and 30 %, and all reach 75 % of the volume of pores with a diameter about 250 μm and 100 % at 1000 μm. In contrast, *T* samples have more diversity; *T*1_1 starts about 10 %, *T*1_2 at 50 % and the remaining T samples are between 20 and 40 %. The group within *T* that seems to show less variability is *T*3, where 75 % is reached in about 200–250 μm. The *T*1 group shows the singular behavior of the sample *T*1_1; this sample does not reach 100 % of the pores until it reaches a diameter of 1,470 μm. The sample *T*1_2 has a singularity; it appears to lack pores between 30 and 150 μm, there is an abrupt change making the curve not grow in the same smooth way as the rest. *T*2 samples are grouped into two behaviors, one starting at 20 % and another at 40 %.

Table 4 shows statistical results of the Kolmogorov–Smirnov test that compares two sample distributions. Comparisons of all possible pairs of data are shown. Bold type and shading highlight pairs of samples with a statistically significant difference for a confidence level of 95 % or higher. It can be seen that sample *T*1_1 is statistically different from all others; the rest of the statistical differences are mostly between *T* and *N* samples. Not taking sample *T*1_1 into account, there are 37 of 110 pairs of samples statistically different between groups, and within the same group (either *N* or *T*) there are four pairs of samples statistically different from the 100 possible. Furthermore, differences between *N* and *T* samples seem to correlate with depth, and so there are 23 over 40 in *N*1, 16 over 40 in *N*2 and 5 over 30 in *N*3.

Table 5

*Mean squares (MS) of the multifactorial ANOVA analysis with * if $P < 0.1$, ** if $P < 0.05$ and *** if $P < 0.01$*

	Porosity	POM	Total pore surface	Specific pore surface	Total pore connectivity	Specific pore connectivity
Soil use	23.836*	0.033*	3.69E7***	412.162*	2.18E + 6	181,017.000**
Depth	0.421	0.000	3.59E + 7	4.295	1.43E + 6	36,234.600

4.4. *Effects of Soil Use and Depth*

Table 5 shows the mean squares values for the multifactorial ANOVA analysis. The value of total pore surface has a P value <0.05 suggesting that factor treatment produces a statistically significant difference for this variable. Furthermore, the difference in specific pore connectivity between T and N samples is also statistically significant.

5. *Summary and Conclusions*

This work shows the utility of performing different geometric measures of soil pore space using 3D images in order to characterize the soil structure. We characterized in quantitative terms several geometric factors of great interest in the study of biological and physical processes, such as porosity, pore surface area, connectivity of the pores and pore size distribution. For this latter purpose, we needed to use tools of mathematical morphology, which reflect almost perfectly pore size criteria (Vogel, 2002). Measurements were made directly on the samples without altering them, this being an advantageous technique employed by further research. Our comparisons indicate total pore surface and specific pore connectivity show the greatest differences between the two soil types (natural vegetation and tillage). Iin addition, we quantified the relationships between different geometric measurements for all soil samples demonstrating that most of them are related via high correlation coefficients.

Acknowledgments

This research work was partially funded by Spain's Plan Nacional de Investigación Científica, Desarrollo e Innovación Tecnológica (I + D + I) under ref. AGL2011-25175.

References

Brewer, R. 1964 Fabric and mineral analysis of soils. John Wiley and Sons.

Brye, K.R., and A.L. Pirani. 2005 *Native soil quality and the effects of tillage in the grand prairie region of eastern Arkansas.* Am. Midl. Nat. *154*, 28–41. doi:10.1674/0003-0031(2005)154[0028:NSQATE]2.0.CO;2.

Chun, H.C., D. Giménez, and S.W. Yoon. 2008 *Morphology, lacunarity and entropy of intra-aggregate pores: Aggregate size and soil management effects.* Geoderma *146*, 83–93. doi:10.1016/j.geoderma.2008.05.018.

Dathe, A., Tarquis, A.M., and Perrier, E. 2006 *Multifractal analysis of the pore-and solid-phases in binary two-dimensional images of natural porous structures.* Geoderma *134*(3), 318–326.

Dexter, A.R. 1988 *Advances in characterization of soil structure.* Soil Till. Res. *11*, 199–238.

Gale, W.J., Cambardella, C.A. 2000 *Carbon dynamics of surface residue and root-derived organic matter under simulated no-till.* Soil Sci. Soc. Am. J. *64*, 190–195.

Gantzer, C.J., Anderson, S.H. 2002 *Computed tomographic measurement of macroporosity in chisel-disk and no-tillage seedbeds.* Soil Till. Res. *64*, 101–111.

Gibson, J.R., Lin, H., Bruns, M.A. 2006 *A comparison of fractal analytical methods on 2- and 3-dimensional computed tomographic scans of soil aggregates.* Geoderma *134*, 335–348.

Glasbey, C. A. and Horgan, G. W. 1995 Image Analysis for Biological Sciences. John Wiley and Sons. Chichester, England.

Iassonov, P., Gebrenegus, T., and Tuller, M. 2009 *Segmentation of X-ray computed tomography images of porous materials: A crucial step for characterization and quantitative analysis of pore structures.* Water Resources Research *45*(9).

INIA. 1977 El Encín, suelo y clima. INIA-MAPA, Madrid, 213 pp.

Kravchenko, A.N., Wang, W., Smucker, A.J.M., Rivers, M.L. 2011 *Long-term differences in tillage and land use affect intra-aggregate pore heterogeneity.* Soil Sci. Soc. Am. J. *75*, 1658–1666.

Lal, R. 2002 *Soil carbon dynamics in cropland and rangeland.* Environ. Pollut. *116*, 353–362.

Michielsen, K., De Raedt, H. 2001 *Integral-geometry morphological image analysis.* Physics Reports *347*(6), 461–538.

Nunan, N., Ritz, K., Rivers, M., Feeney, D.S., Young, I.M. 2006 *Investigating microbial micro-habitat structure using X-ray computed tomography.* Geoderma *133*, 398–407.

Peth, S., Horn, R., Beckman, F., Donath, T., Fisher, J., Smucker, A.J.M. 2008 *Three-dimensional quantification of intra-aggregate*

pore space features using synchrotron radiation-based microtomography. Soil Sci. Soc. Am. J. *72*, 897–907.

Posadas, A.N.D., Giménez, D., Quiroz, R., Protz, R. 2003 *Multifractal characterization of soil pore systems*. Soil Science Society of America Journal *67*, 1361–1369.

Revil, A., Cathles, L.M. 1999 *Permeability of shaly sands*. Water Resour. Res. *35*, 651–662.

Rasband, W. S. 1997 ImageJ, US National Institutes of Health, Bethesda, Maryland, USA.

Saucier, A., Muller, J. 1999 *Textural analysis of disordered materials with multifractals*. Physica A *267*, 221–238.

San José Martínez. F., M.A. Martín, F.J. Caniego, M. Tuller, A. Guber, Y. Pachepsky, C. García-Gutiérrez. 2010 *Multifractal analysis of discretized X-ray CT images for the characterization of soil macropore structures*. Geoderma *156*, 32–42.

San José Martínez, F., F.J. Muñoz, F.J. Caniego, F. Peregrina. 2013 *Morphological Functions to Quantify Three-Dimensional Tomograms of Macropore Structure in a Vineyard Soil with Two Different Management Regimes*. Vadose Zone J. *12*(3).

Serra, J. 1982 Image analysis and mathematical morphology. Academic Press Inc. Orlando, Florida, USA.

Six, J., Paustian, K., Elliott, E.T., Combrink, C. 2000 *Soil structure and organic matter. I. Distribution of aggregate-size classes and aggregate associated carbon*. Soil Science Society of America Journal *64*(2), 681–689.

Soil Survey Staff. 2010 Keys to Soil Taxonomy, 11th ed. USDA-Natural Resources Conservation Service, Washington, DC.

Vogel, H. J. 2002 Topological characterization of porous media. In Morphology of condensed matter (pp. 75–92). Springer Berlin Heidelberg.

Wang, W., Kravchenko, A.N., Smucker, A.J.M, Rivers, M.L. 2012 *Intra-aggregate pore characteristics: X-ray computed microtomography analysis*. Soil Sci. Soc Am J *76*, 1159–1171.

Young, I.M. and Crawford, J.W. 2004 *Interactions and self-organization in the soil–microbe complex*. Science *304*(5677).